Dynamic translation regulation in *Caulobacter* cell cycle control

Jared M. Schrader[a,1,2], Gene-Wei Li[b,3], W. Seth Childers[a,4], Adam M. Perez[a,5], Jonathan S. Weissman[b,c], Lucy Shapiro[a,2], and Harley H. McAdams[a,2]

[a]Department of Developmental Biology, Stanford University, Stanford, CA 94305; [b]Department of Cellular and Molecular Pharmacology, California Institute of Quantitative Biology, Center for RNA Systems Biology, University of California, San Francisco, CA 94158; and [c]Howard Hughes Medical Institute, University of California, San Francisco, CA 94158

Contributed by Lucy Shapiro, September 8, 2016 (sent for review July 27, 2016; reviewed by Bert Ely and Jeffrey W. Roberts)

Progression of the *Caulobacter* cell cycle requires temporal and spatial control of gene expression, culminating in an asymmetric cell division yielding distinct daughter cells. To explore the contribution of translational control, RNA-seq and ribosome profiling were used to assay global transcription and translation levels of individual genes at six times over the cell cycle. Translational efficiency (TE) was used as a metric for the relative rate of protein production from each mRNA. TE profiles with similar cell cycle patterns were found across multiple clusters of genes, including those in operons or in subsets of operons. Collections of genes associated with central cell cycle functional modules (e.g., biosynthesis of stalk, flagellum, or chemotaxis machinery) have consistent but different TE temporal patterns, independent of their operon organization. Differential translation of operon-encoded genes facilitates precise cell cycle-timing for the dynamic assembly of multiprotein complexes, such as the flagellum and the stalk and the correct positioning of regulatory proteins to specific cell poles. The cell cycle-regulatory pathways that produce specific temporal TE patterns are separate from—but highly coordinated with—the transcriptional cell cycle circuitry, suggesting that the scheduling of translational regulation is organized by the same cyclical regulatory circuit that directs the transcriptional control of the *Caulobacter* cell cycle.

Caulobacter | cell cycle | translation | regulation | ribosome profiling

The *Caulobacter crescentus* cell cycle produces two daughter cell types at each cell division: a nonreplicative motile swarmer cell, and a replication-competent sessile stalked cell. At the time of the asymmetric cell division, each daughter cell activates a different genetic program. *Caulobacter* has a cyclical genetic circuit that controls the varying temporal and spatial expression of multiple functional modules (Fig. 1) that implement biogenesis of polar organelles, replication and segregation of the chromosome, and cytokinesis (1–4). The circular 4-Mb genome has 3,885 ORFs and 199 noncoding RNAs (5, 6). mRNA profiling by microarrays or RNA-seq (7–10) and global promoter activity profiles from 5′ Global RACE experiments (11) have shown that several hundred *Caulobacter* mRNAs have significant temporal transcriptional variation over the cell cycle. The expression of cell cycle-controlled mRNAs largely correlates with the times they are required for the functional modules that implement progression of the cell cycle (8). The transcriptional activity of most of the *Caulobacter* cell cycle-regulated promoters is controlled by a genetic circuit comprised of four transcriptional master regulators, a DNA methyltransferase (2), and a dynamic set of polar-localized phospho-signaling proteins that control asymmetric cell division (12–15). Because regulation of translation has an immediate impact on protein production, a major cellular energy drain, tight regulation of translation is essential for rapid cell adaptation to changing circumstances. In eukaryotic cells translational control is known to regulate cell cycle transitions (16–18), but the global role for translational control of the bacterial cell cycle has remained largely unexplored. We have used ribosome profiling (19) to determine the global role of translational regulation in differential protein production during the *Caulobacter* cell cycle. We measured translational efficiency (TE), the ratio of ribosome profiling (RP level)/RNA-seq (RS level) (*Materials and Methods*), which reflects the relative rate of protein production from each mRNA and thus provides a metric for translational regulation of protein production from each gene (19, 20). Prior studies have shown that operons which encode multiprotein complexes often modulate TE so that ORFs within the operon are differentially translated to match the stoichiometry of the proteins in the complex (20, 21). The observed organization of genes that encode proteins that work together into operons with differential TE between genes in the operon is an evolutionarily selected strategy for enhancing robustness against transcription-level stochastic gene expression (20, 22). Analyses of differential TE in bacterial operons revealed a strong correlation between codon use in ORFs and the corresponding protein stoichiometry in complexes involving the proteins they encoded (23). However, these studies only investigated the average levels of operon translation in mixed-cell populations, rather than the relation

Significance

The *Caulobacter* cell cycle is controlled by a genetic circuit that dynamically regulates transcription of nearly 20% of the genome; however, the role of translational control of cell cycle progression is unexplored. To understand the contribution of translational regulation, we measured both mRNA and translation levels at multiple stages of the cell cycle. We found that cell cycle-dependent translational regulation is important for hundreds of genes and also that the positioning of regulatory proteins to a specific cell pole is coordinated by the timing of their synthesis. The cell cycle-regulatory pathway that controls translation rates is linked to the regulatory circuit that controls transcription rates of cell cycle-regulated genes.

Author contributions: J.M.S., G.-W.L., J.S.W., and L.S. designed research; J.M.S., W.S.C., and A.M.P. performed research; J.M.S. and H.H.M. analyzed data; and J.M.S., L.S., and H.H.M. wrote the paper.

Reviewers: B.E., University of South Carolina; and J.W.R., Cornell University.

The authors declare no conflict of interest.

Data deposition: The data reported in this paper have been deposited in the Gene Expression Omnibus (GEO) database, www.ncbi.nlm.nih.gov/geo (accession no. GSE68200).

[1]Present address: Department of Biological Sciences, Wayne State University, Detroit, MI 48202.

[2]To whom correspondence may be addressed. Email: shapiro@stanford.edu, hmcadams@stanford.edu, or schrader@wayne.edu.

[3]Present address: Department of Biology, Massachusetts Institute of Technology, Cambridge, MA 02139.

[4]Present address: Department of Chemistry, University of Pittsburgh, Pittsburgh, PA 15260.

[5]Present address: Department of Molecular and Cell Biology, University of California, Berkeley, CA 94720.

This article contains supporting information online at www.pnas.org/lookup/suppl/doi:10.1073/pnas.1614795113/-/DCSupplemental.

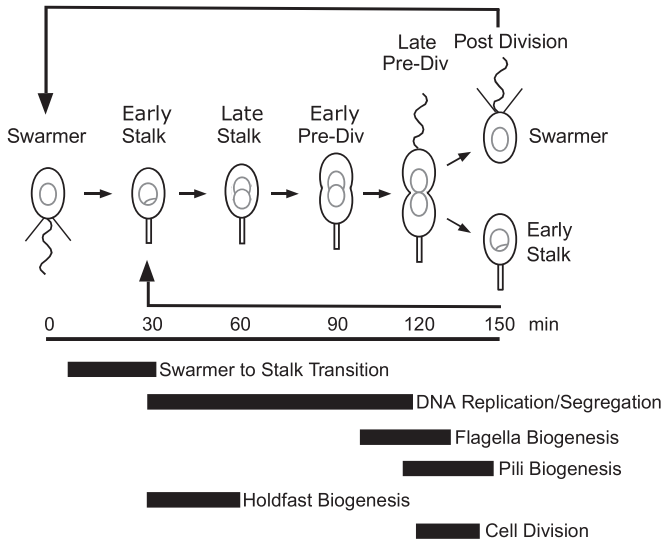

Fig. 1. *Caulobacter* cell cycle. Black bars below indicate intervals of cell cycle functions. At 30-min intervals, samples were collected for the RS and RP assays. Over the course of the cell cycle, pili (straight lines) and a flagellum (wavy line) are generated and then discarded. A stalk (straight protrusion) grows on the site of the discarded flagellum. The chromosome and its progressive replication are indicated by the gray figures within the cells. Arrows indicate how the stalk and swarmer cells reenter the cell cycle.

between timing of protein production and assembly of the complexes within synchronized cell populations.

Here we explore the global patterns of *Caulobacter* transcription and translation, particularly the role of dynamic translational regulation in implementation of the cell cycle. By clustering the TE profile over the cell cycle we identify several hundred genes that have strong cell cycle-dependent translational regulation (Dataset S1). The temporal patterns of TE variation fell into a relatively small number of distinct patterns. Notably, we found that the temporal control of translation provides a mechanism for restricting the positioning of regulatory proteins to a specific cell pole. In addition, comparison of the RS and TE profiles suggests many *Caulobacter* genes have coordinated, but distinct, transcriptional and translational regulatory pathways that modulate the temporal control of cell cycle-regulated genes.

Results

We synchronized *C. crescentus* (strain NA1000) cells and collected six samples at 30-min intervals over the cell cycle. For each sample, we assayed RS normalized reads per kilobase per million mapped reads (RS RPKM) to determine relative mRNA levels and RP normalized read counts (RP RPKM) to determine relative translational activity (19, 21, 24). We removed genes where either the RS or RP data series had 0 raw read counts in any sample, leaving 3,048 genes. We determined relative transcriptional and translational activity of these ORFs at each of the six time points in terms of the normalized sequencing read counts that mapped to that ORF. For RS, the normalized read count mapping to an ORF is proportional to the number of the corresponding mRNAs present. The RP normalized read counts mapped to an ORF are proportional to the number of ribosomes bound to the corresponding mRNA and, because virtually all ribosomes complete translation of the mRNA, also to the number of proteins being synthesized from that ORF (20, 21). With the exception of rapidly proteolysed proteins, this measure is also strongly correlated with the number of proteins present in the cell (21).

Global Characteristics of *Caulobacter* Transcription and Translation. The cumulative distribution of averaged RS and RP RPKM (Fig. 2*A*) shows that a relatively small number of genes are responsible for the majority of RS RPKM and of RP RPKM at any given time. The cumulative distribution for the averaged RPKM (representing a mixed or nonsynchronized cell population) shows that 300 genes produce 60% of the RS RPKM and 68% of the RP RPKM; however, the sets of genes with the most RS and RP RPKM are not identical. Fig. 2*B* shows the cumulative distribution of RS RPKM for each cell cycle time point sample. For the $T = 0$-min sample (swarmer cell), the 300 genes with highest RS RPKM account for 55% of the RS RPKM

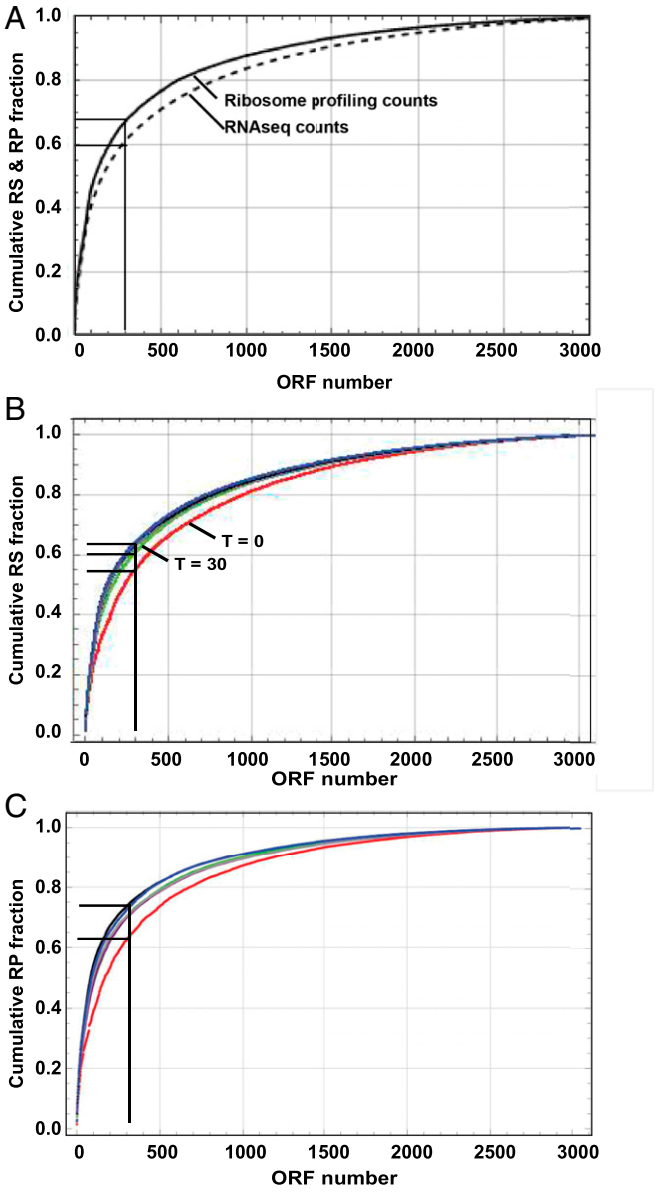

Fig. 2. Cumulative fractional distribution of averaged RS and RP RPKM. (*A*) Solid line: Cumulative fractional distribution of ribosome profiling RPKM averaged over six time samples. Dashed line: Cumulative fractional distribution of RS RPKM averaged over six time samples. (*B*) Cumulative fractional distribution of RS RPKM for each of the six time samples. The fraction of the counts in the 300 most highly expressed genes increases substantially between the $T =$ 0-min sample (red) and the $T = 30$-min sample (green). (*C*) Cumulative fractional distribution of RP RPKM for each of the six time samples.

(55%), whereas at $T = 30$ min and later, the distribution changes so that a larger fraction (60–64%) of the total RS RPKM arises from the 300 most highly transcribed genes. A histogram of the changes in RS RPKM over the gene population (*SI Appendix*, Fig. S1) shows a roughly symmetric distribution of increases and decreases in RS RPKM from $T = 0$ to $T = 30$ min. However, examination of the 150 genes most strongly up- and down-regulated (*SI Appendix*, *List L1*) shows a dramatic change in the composition of the highly expressed gene population: genes associated with the flagellum, pilin, and chemotaxis are strongly down-regulated in this interval, whereas genes associated with cell growth (especially ribosome- and cell wall-associated proteins) are strongly up-regulated. *SI Appendix*, *List L1* also shows the genes whose mRNA (RS RPKM) is most strongly up- and down-regulated in the intervals $T = 30$ to $T = 60$ min and $T = 60$ to $T = 90$ min. The worksheet "Delta RP vs interval" in Dataset S2 has comparable information for RP RPKM changes. These results show that there are ongoing major changes in the composition of the highly expressed gene population as the cell cycle progresses (we do not include the changes in later cell cycle samples, as they begin to include values from next-generation daughter cells along with the late-predivisional cells).

Fig. 2*C* shows that the cumulative RPKM distribution curves for RP are comparable to the RS RPKM shown in Fig. 2*B*. Note that the RP RPKM are even more concentrated into a few highly translated genes than the RS RPKM. Below we discuss results from clustering the TE profiles of ~500 genes with highest protein production. Fig. 2*C* shows that this group of genes comprises about 80% of the cell's protein production. The histogram of the average TEs for 3,048 genes (*SI Appendix*, Fig. S2) shows that 90% of the genes have average TE between 0.4 and 2.0. *SI Appendix*, Fig. S3 shows average RP plotted versus average RS for genes with average RP > 100; the average TE of these genes is 1.35. As previously observed for multiple bacterial operons (6, 23), we find that the temporal average TE generally varies widely over the genes in operons as, for example, with the *Caulobacter sciP* operon genes (*SI Appendix*, Fig. S4).

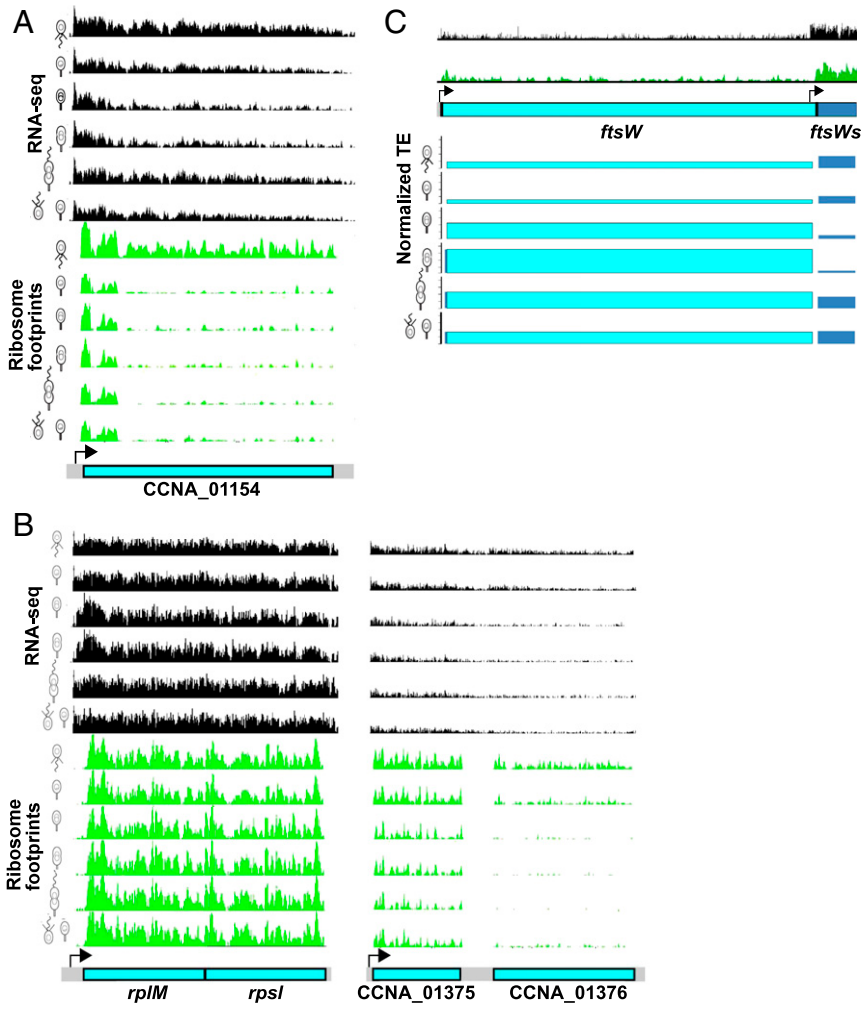

Fig. 3. Three examples of diverse modes of translational regulation. Cell cycle stage is indicated by the small icons to the left. (*A*) Differential elongation of the CCNA_01154 protein as a function of cell cycle progression. The distributions of RNA-seq read density (black) and ribosome footprint read density (green) are shown. Ribosome occupancy drops off strongly past codon 29 after the swarmer cell stage, possibly because of translation termination at this point or slow translation progression after this point. (*B*) Ribosome footprint read density (green) and RNA-seq read density (black) for two operons. The *rplM/rpsI* ribosomal protein operon has a constant TE throughout the cell cycle. The ORFs encoded in the CCNA_01375/CCNA_01376 operon (6) exhibit different levels of ribosome occupancy as a function of the cell cycle, with the highest level of translation in the swarmer and early stalked cells. (*C*) Differential expression of the cell division gene *ftsW* protein isoforms. The *ftsW* gene is transcribed in two forms, a lowly transcribed form leading to the translation of a full-length protein and a highly transcribed form leading to the translation of a small 36-amino acid peptide in the same reading frame (6).

Three Examples of Translational Regulation. Fig. 3*A* shows the RS and RP data for the conserved hypothetical gene CCNA_01154, which encodes a C-terminal DNA endonuclease domain. There are cell cycle-dependent changes in the ribosome density along the CCNA_01154 ORF with ribosomes present on the full length of the mRNA only in the swarmer cell. Thereafter in the cell cycle, the ribosome occupancy drops dramatically after the 29th codon. This finding suggests there is cell cycle-dependent regulation of the ribosome elongation rate or translation termination for this gene. In Fig. 3*B*, the 50S ribosomal subunit protein L13 *rplM*/*rpsI* (CCNA_01440/CCNA_01441) operon has near constant RS, RP, and TE throughout the cell cycle. In contrast, both ORFs in the CCNA_01375/CCNA_01376 operon exhibit cell cycle-dependent changes in RP. CCNA_01376, encoding a putative glutathione *S*-transferase, has a substantial decrease in RP RPKM over the cell cycle, whereas CCNA_01375 has a much smaller decrease. The TE of CCNA_01375, encoding a putative lactoylglutathione lyase, has relatively small variation (1.90–1.55), whereas CCNA_01376 has a larger variation (1.09–0.50). Fig. 3*C* shows *ftsW*, a gene with an internal promoter that drives expression of a short 36-amino acid isoform of the FtsW protein (6). The two FtsW isoforms exhibit differential translational regulation: The N-terminal portion of the mRNA encoding the full-length protein has a fourfold variation in TE peaking in the early predivisional cell, whereas the short form undergoes a twofold variation that is lowest in the early predivisional cell. These three examples illustrate the flexibility and diversity of the bacterial cell's dynamic transcriptional and translational regulatory mechanisms.

Patterns of Translational Regulation. Among genes with the largest cell cycle variation in TE, similar profiles are found across many groups of genes, which in many instances include subsets of genes in an operon. Independent of the operon structure, some groupings of genes and subsets of operons have internally consistent RS and consistent TE temporal profiles, but the common RS and TE profiles in these cases sometimes differ from each other. For example, the eight-gene *sciP* operon has at least two distinct RS profiles (Fig. 4*A*) (CCNA_00948-00949 and CCNA_00951-00956), and three different TE profiles (CCNA_00948, CCNA_949-950, and CCNA_00951-00956). The *fliL* operon (Fig. 4*B*) has a similar diversity of RS and TE cell cycle profiles.

Fig. 5 shows three sets of functionally related genes involved in polar morphogenesis and chemotaxis. The 12-gene chemotaxis operon (CCNA_00439-00450) (Fig. 5*A*) has nearly consistent RS and TE profiles over the cell cycle. In contrast, in Fig. 5*B* the 10 stalk-related genes, consisting of two multigene operons plus four single genes, exhibit three distinct RS-TE profiles, all involved

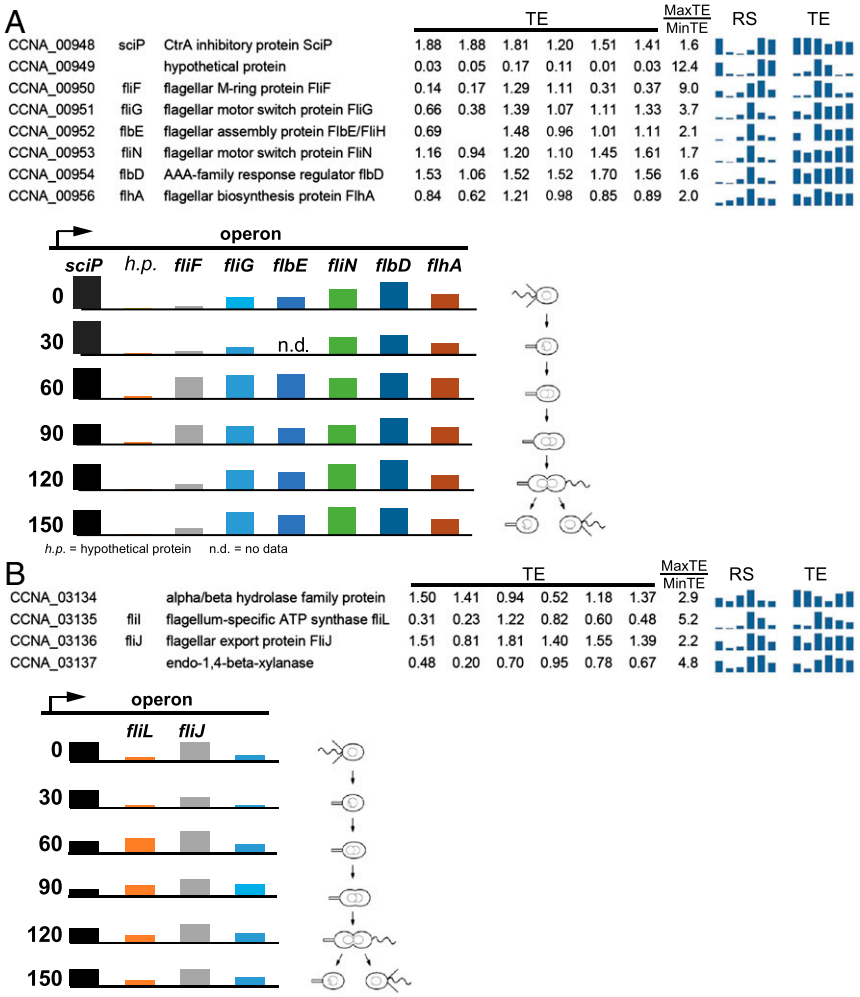

Fig. 4. Translational regulation in the SciP (*A*) and FliLJ (*B*) operons. Each panel shows the genes in an operon. The minibar charts at right are normalized to the highest value to show the temporal regulatory patterns. The height of the colored bars in the operon diagrams are proportional to the TE value for each gene. TE values for the genes in each operon vary independently as the cell cycle progresses.

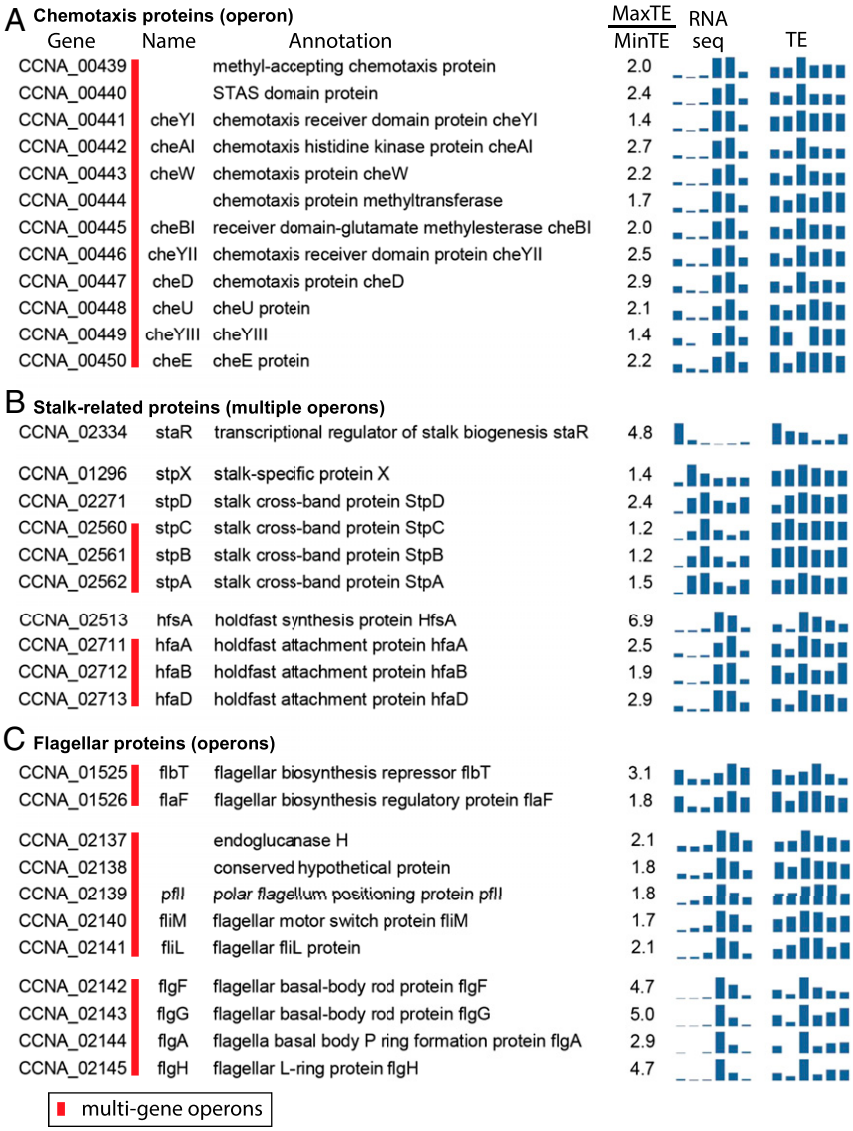

Fig. 5. Proteins encoding multiprotein complexes with ordered assembly pathways show different patterns of coordinated transcriptional and translational regulation. (*A*) Twelve chemotaxis proteins in a single operon show a similar regulatory pattern. Missing bars in the graph for *cheYIII* and *flgA* result from missing data points. (*B*) Ten stalk-related proteins have three distinct regulatory patterns and an eclectic operon organization. (*C*) Eleven flagellar proteins organized into three operons each with a distinctive regulatory pattern.

in a cascade that controls stalk biogenesis. The ordering of the different RS peaks in the three groups follows the order of stalk assembly (25, 26). The second gene group (CCNA_01296-02562) shows comparable profiles for genes in three separate operons; the third gene group also shows comparable RS-TE profiles across operons, but it is a different profile from the second group. The 11 flagellar proteins in Fig. 5*C* are in three operons whose expression patterns fall into two TE profiles (CCNA_01525-01541 and CCNA_02142-02145) and two disjointed RS profiles (CCNA_01525-01526 and CCNA_02137-02145). The operon CCNA_02142-02145 shows a TE profile that is distinct from the other two operons in Fig. 5*C*. In all cases in Fig. 5, the RS and TE profiles are each internally consistent, while differing from each other. The stalk and flagellar proteins are each required for assembly of the two structures at specific times in the cell cycle. In each of these cases, the respective operon proteins are required in a particular temporal order to create the structure. The chemotaxis proteins are also needed at a specific time in the cell cycle, but without the strong ordering requirement. These various functional requirements are strongly reflected in the RS and TS regulatory profiles shown.

Clustering Identifies Genes with Distinctive TE Patterns over the Cell Cycle. We selected 484 genes with: (*i*) RP RPKM >100 in each sample, (*ii*) ratio of (maximum TE)/(minimum TE) > 1.5, and (*iii*) relatively low noise in the TE profile (by low-pass filtering). (The maximum and minimum in the Max/Min ratio being within the six sample times for each gene.) We clustered the normalized TE profiles of these 484 genes into 14 clusters using a *k*-means algorithm (Dataset S1). The last two columns on the right of the cluster table have normalized minibar charts of the temporal profiles of the RS RPKM and TE. Fig. 6 contains a sample of the clusters from the full cluster table (Dataset S1), which is too large to include here. Observations from comparison of profiles in Dataset S1 include: (*i*) cell cycle-dependent translational regulation (i.e., translational efficiency or TE) for several hundred genes; (*ii*) a relatively small number of distinctive TE patterns; (*iii*) the RS and TE profiles are more strongly correlated in the

CCNA No	Name	Annotation	Avg RS	Avg RP	Max/Min TE	Clust. No	RNA-seq	TE
CCNA_01324	rpmD	LSU ribosomal protein L30P	3982	1444	2.72	2		
CCNA_02420	exbD	TonB accessory protein exbD	5090	1743	2.28	2		
CCNA_01527	fljL	flagellin fljL	1398	1252	8.97	3		
CCNA_00530		LSU ribosomal protein L10P	6942	4963	2.36	3		
CCNA_02419	tonB1	TonB1 protein	4515	2229	2.35	3		
CCNA_01058		helix-turn-helix transcriptional regulator	1566	706	2.24	3		
CCNA_02277		TonB-dependent outer membrane channel	353	632	5.62	4		
CCNA_00835	fljN	flagellin FljN	443	743	5.45	5		
CCNA_03972		hypothetical protein	1269	2656	4.33	5		
CCNA_03919		hypothetical protein	2908	4185	3.14	5		
CCNA_02274		EF-Hand domain protein	307	663	2.61	5		
CCNA_03639		ferredoxin, 2Fe-2s	374	866	2.48	5		
CCNA_03012		peroxiredoxin	1342	1291	2.44	5		
CCNA_03060		conserved hypothetical protein	743	1461	2.20	5		
CCNA_03995		hypothetical protein	1607	1572	2.05	5		
CCNA_03303		translation elongation factor Tu (EF-TU)	543	1492	2.02	5		
CCNA_03224		hypothetical protein	801	621	2.84	6		
CCNA_00124		conserved hypothetical protein	915	656	2.56	6		
CCNA_03091		hypothetical protein	661	870	2.25	6		
CCNA_01386		conserved hypothetical protein	620	657	2.22	6		
CCNA_02047		glutamine synthetase	1298	3738	4.27	9		
CCNA_03325		hypothetical protein	3058	9193	3.65	9		
CCNA_01601		conserved hypothetical protein	345	885	2.17	9		
CCNA_01074		entericidin B-like protein	326	949	2.15	9		
CCNA_00808		LSU ribosomal protein L34P	10548	26575	2.12	9		
CCNA_00802	ybgT	cyd operon protein YbgT	514	1564	3.35	11		
CCNA_03933		hypothetical protein	2779	12350	3.04	11		
CCNA_02931		flgE-related flagellar hook protein	703	921	2.91	11		
CCNA_03932		hypothetical protein	2697	9438	2.68	11		
CCNA_03400		conserved hypothetical protein	911	2235	2.24	11		
CCNA_03997		amelogenin/CpxP-related protein	718	1503	2.22	11		
CCNA_00371		ATP synthase B' chain	1262	903	2.04	12		
CCNA_00320		LSU ribosomal protein L27P	6360	5354	2.02	12		

Fig. 6. A subset of the genes in the clusters in Dataset S1 with RP (RPKM) > 600. The missing bar in the graph for CCNA_03932 results from a missing data point. Readers are encouraged to view the clusters in the complete dataset in Dataset S1.

clusters (e.g., 1–4 and 6) that have on average larger MaxTE/MinTE ratios; and (*iv*) clusters with relatively low MaxTE/MinTE ratios (e.g., 13 and 14) show much less RS-TE profile correlation.

Dramatic Cell Cycle-Dependent Changes in the Cell's Protein Complement. The changes in the RP RPKM between our temporal samples show alterations in the cell's protein synthesis priorities as the cell cycle progresses (see Dataset S2 "Delta RP versus interval" worksheet). There is a strong increase in production of ribosomal proteins during the swarmer-stalk transition ($T = 0$ to $T = 30$ min) and in early stalked cell development ($T = 30$ to $T = 60$ min). Production of proteins needed for the upcoming large-scale production of new cell wall (e.g., the RsaA S-layer protein and components of the TonB-dependent receptor complexes) is also notably increased. In the $T = 0$ to $T = 30$-min interval, production of numerous proteins is also greatly reduced, notably including proteins associated with the pili, flagellum, and chemotaxis subsystems. There is no correlation between the increases in transcription and the average TE over $T = 30$ and $T = 60$ min (*SI Appendix*, Fig. S5).

It is of interest that cluster 3 of the genes with strong TE regulatory profiles contains seven ribosomal protein genes where the TE increases significantly in the sample period just before the increase in RS (Dataset S1). Similarly, Fig. 5 shows three examples for chemotaxis, holdfast, and flagellar genes where TE increases before a significant increase in RS for genes. It does seem reasonable that increasing TE before an increase in transcription could be an efficient strategy to ensure that translation machinery is available when mRNAs are produced. Just as these genes in Fig. 5 are considered to be transcriptionally coregulated genes, they must also be considered to be translationally coregulated.

A similar pattern is observed in the divisome proteins that are components of the cell-division machine (27). Of 23 divisome proteins, 5 (FzlA, FtsQ, FtsK, FtsL, and FtsB) have this characteristic (worksheet "Divisome Genes" in Dataset S2). These five proteins arrive at the division plane over 25 min: first FzlA, then in 15 min FtsQ, FtsK, and FtsL, then after another 10 min, FtsB (see figure 4B in ref. 27). In the case of FtsQ, FzlA, and FtsK, TE clearly increases before the increase in RS, reflecting the anticipatory translational regulatory pattern noted above. These distinct and coordinated RS and TE maxima over the cell cycle are presumably the result of selection for efficient protein production.

SpmX Is Synthesized in the Swarmer Cell for Immediate Localization to the Cell Pole. In *Caulobacter* cells protein complexes of different composition are assembled at opposite cell poles where they control cell-type–specific functions, including signaling protein-mediated differential expression of the genome after cell compartmentalization and MipZ-directed positioning of the divisome (12, 13, 15, 28–31). During the swarmer to stalked cell transition, the protein complex of the formerly flagellated pole is replaced by the proteins required at a stalked pole protein complex. The SpmX polar protein localization factor and bactofillin BacB synthesis is timed so that both RS and RP levels peak in the swarmer stage, whereas the other proteins are most strongly produced later in the early stalked cell phase (Dataset S1). Thus, the cell uses both transcriptional and translational control to produce these proteins when needed and in the needed quantities. The polar protein assembly factor PopZ has two TE peaks; the first in the swarmer cell is coincident with the synthesis of stalk pole localization factor SpmX, and the second in the stalked cell is coincident with synthesis of the swarmer pole localization factor PodJ (Dataset S1).

We investigated the timing and positioning of one of these polar proteins, the SpmX localization factor. SpmX is a component of the signaling complex that is positioned at that the stalked pole during the swarmer-to-stalked cell transition (28, 30) (Fig. 7*A*). Both transcription and translation of *spmX* are strongly activated in the swarmer cell, and SpmX is then immediately localized to the stalked pole (30), where it binds directly to the polar PopZ polymeric matrix (28). As the cell cycle

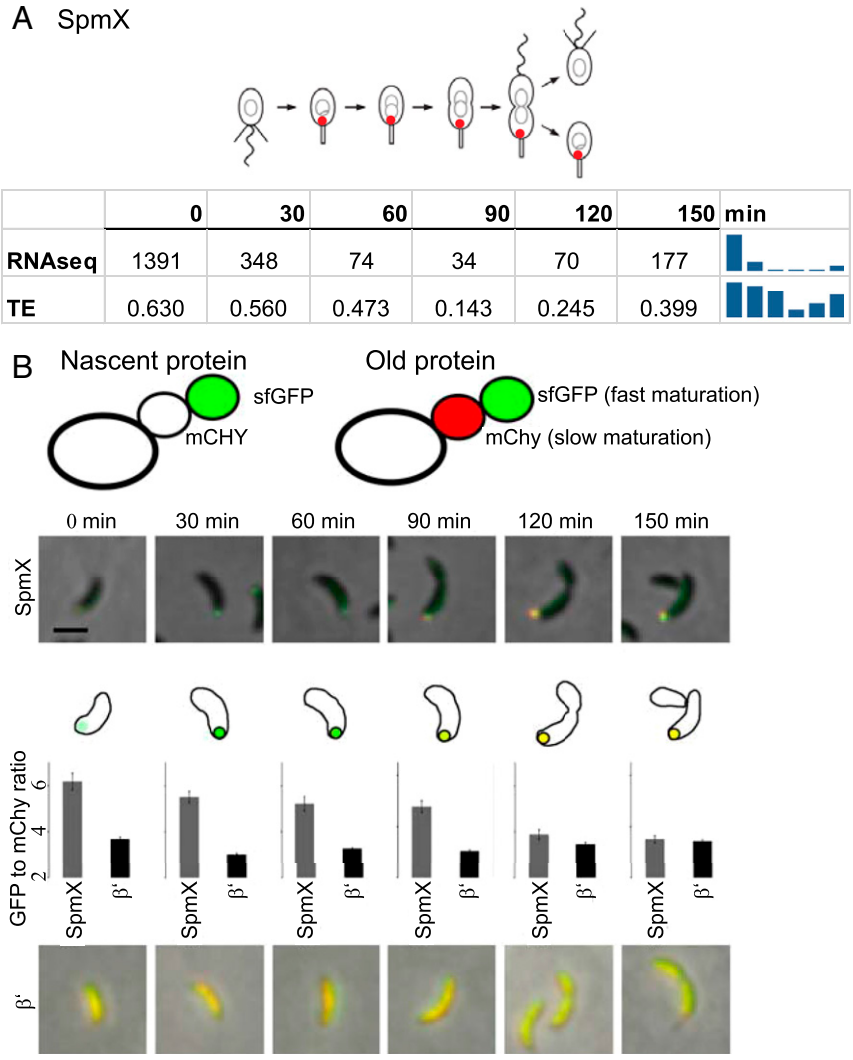

Fig. 7. Coordinated transcription and translation of *spmX* assures that SpmX is only present for localization to the stalk cell pole. (*A*) Polar position of SpmX (red) as cell cycle progresses. Table: RS RPKM and TE. Minibar charts (*Right*) show RS and TE levels. (*B*) Nascent SpmX protein is localized to the pole. A fluorescent timer cassette has slow-folding mCherry (mChy, red) and fast-folding superfolder GFP (green) fused to SpmX. Control: C terminus of the constitutively expressed β′ subunit of RNA polymerase fused to the timer cassette. Fluorescent images of sfGFP and mCherry signals are shown. (Scale bar, 2 μM.) Yellow: Overlapping red and green signals. Bar graphs: Average GFP to mCherry ratio at the cell cycle time points.

progresses, a second PopZ matrix is established at the pole opposite the stalked pole. Importantly, SpmX is synthesized in the nascent stalked cell only when the PopZ matrix is present at the stalked pole, which assures that SpmX is localized to the correct pole. This multiprotein complex at the stalked pole is central to the asymmetric signaling cascade that yields the differentiated swarmer and stalk cells at the next cell division (12).

To confirm that the time of *spmX* mRNA translation corresponds to the time of formation of the stalked pole complex, we attached two tandem fluorophores to the C terminus of SpmX, a slow-maturing mCherry and a fast-maturing superfolder GFP (sfGFP), to create a fluorescent "timer" (Fig. 7*B*). This construct enables identification of newly synthesized SpmX proteins by differentiating the sfGFP and the mCherry signals (32). As a control, we fused the C terminus of the constitutively expressed β′ subunit of RNA polymerase to the fluorescent timer. The maximum SpmX sfGFP-to-mCherry signal ratio occurred in the swarmer cell (Fig. 7*B*) corresponding to the burst of transcription, indicating that SpmX is made immediately and quickly localized to the stalked cell pole (Fig. 7*A*). The GFP-to-mCherry signal ratio gradually dropped throughout the cell cycle, reaching a minimal value at 150 min, because of the additional time required for mCherry to mature (Fig. 7*B*). For the constitutively produced β′-subunit of RNA polymerase, the ratio of sfGFP-to-mCherry signal remained nearly constant throughout the cell cycle.

Discussion

This work examines the role of coordinated transcriptional and translational control in bacterial cell cycle regulation. Many bacterial translational regulatory mechanisms have been characterized, some global in action and others narrowly targeted (33–35). The cases shown in Figs. 4 and 5 and the clusters in Dataset S1 show that there are *Caulobacter* translational regulatory pathways that produce distinctive globally coordinated and cell cycle-dependent TE profiles. Those cases show that a pathway may provide consistent control of all or part of the genes in operons or consistent control of a disparate group of genes relatively independent of the operon structure. In many cases, particularly for genes with the most distinctive TE changes over the cell cycle, there is a correspondingly distinctive (but not necessarily identical) RS profile. We know that the RS transcriptional cell cycle profiles are coordinated by a well-characterized

cyclical genetic circuit (1, 2, 11, 36). We predict that the timing of pathways driving the TE profiles will be found to be likewise coordinated by regulatory links to elements of that genetic circuit.

Our RS results for small noncoding RNAs are in the worksheet "ncRNA data" in Dataset S2. There are 138 intergenic segments annotated as ncRNAs. Eighteen of these were not expressed under the growth conditions of this experiment. About half of the remaining 120 ncRNAs show a significant cell cycle-dependent expression profile (shown in the "ncRNA data" worksheet in Dataset S2). Transcription factor binding sites upstream were previously identified for 11 of these RNAs (11), and it is intriguing that one or several binding sites for *Caulobacter* master cell cycle regulators are associated with ncRNAs with dynamic cell cycle profiles ("ncRNA data" worksheet in Dataset S2). A search for conserved motifs in the region of the translation start sites was nonproductive. Determination of the connection between these cell cycle-regulated ncRNAs and translational regulation, if any, remains an open question for future investigation.

The example of the timing of SpmX protein synthesis and localization into the stalked pole signaling complex (Fig. 7) shows how the cell coordinates SpmX production with its localization to the stalked pole, and then strongly represses both *spmX* transcription and translation at the time of cell division when the new flagellated polar complexes are being produced. This assures presence of SpmX only at the stalked pole in each cell generation as needed for the proper implementation of asymmetric cell division. Interestingly, another polar protein, the CpaE pili localization factor, exhibits a similarly coordinated transcription and translational regulation, but occurring later in the cell cycle so that CpaE is only inserted into the flagellated cell pole (*SI Appendix*, Fig. S6). In both instances, transcription of the gene peaks sharply near the time when the protein is needed for polar insertion, and translation is relatively repressed except near that time.

Our results demonstrate that *Caulobacter* uses cell cycle-dependent translational regulation that for strongly expressed proteins is generally coordinated with cell cycle-dependent transcriptional regulation. Although we do not identify the molecular mechanisms underlying the observed time-dependent TE profiles, we can infer some general properties of those mechanisms. For example, the respective strong transcriptional (RS) and translational (TE) profiles in each of the TE clusters 1–3, 6, 9, and 11 (Dataset S1) are different from each other but largely consistent for the genes in each cluster. Notably, the clustering was done on the TE temporal profiles, so there was no selection for the transcriptional profiles. As noted above, these coordinated RS and TE temporal patterns suggest that the respective translational regulatory pathways are also driven by a connection to the cyclical genetic circuit that drives the cell cycle-dependent transcriptional regulatory pathways.

In eukaryotic cells, translation is globally regulated by a switch from the canonical scanning mode of translation initiation to an internal ribosome entry site-mediated mode of initiation at the G2/M phase transition (37, 38). To our knowledge, the changes in translation initiation pathways have not been explored as a function of the phases of the bacterial cell cycle. In *Caulobacter* three modes of translation initiation exist: leaderless, leadered Shine–Dalgarno, and nonleadered Shine–Dalgarno (6). We found that mRNAs with moderate affinity Shine–Dalgarno sites have the strongest changes in TE during the cell cycle, whereas leaderless mRNAs and leadered non-Shine–Dalgarno containing mRNAs appear to undergo less dramatic changes in translation (*SI Appendix*, Fig. S7), suggesting that the preferred pathway of translation initiation may be changing during the cell cycle. Indeed, these strongly regulated moderate-affinity Shine–Dalgarno-initiated mRNAs are preferentially translated during the swarmer-to-stalk cell transition (Dataset S1). The protein ratio of translation initiation factors in *Escherichia coli* cells can alter the preferred initiation pathway (39, 40). Notably, the translation patterns of the translation initiation factors themselves all appear to be changing as a function of the cell cycle (Dataset S1), where IF-3 is produced at its highest level during the swarmer-stalk cell transition and IF-2 is produced at its highest level during cell division. This finding suggests that the changing ratio of initiation factor protein levels alters global translation patterns.

It has been proposed that the dominant selective pressure for tight cellular control of protein production rates is the energy cost of synthesizing highly expressed proteins (20, 21). However, the selective pressure to translate proteins, such as SpmX and CpaE, in short time-windows just when they are needed must be driven not only by cellular energy economics, but also by the necessity to avoid harmful effects of mistimed protein production. In each cluster there are genes with high expression levels and others with low expression levels, but with similar RS and TE profiles. How could this come about? Our conjecture is that evolution of the molecular mechanisms that produce particular temporal profiles is primarily driven by the strong selective pressures for tight control of the most highly expressed genes, and then there are fitness advantages—but little energy cost—for lower expressed genes to adopt these mechanisms.

Materials and Methods

Cell Preparation and Synchronization. *Caulobacter* strain NA1000 was grown in minimal growth medium (M2G) (11) and synchronized by isolating swarmer cells (41, 42). Six samples were taken at 30-min intervals over the span $T = 5$ to $T = 150$ min. (In the text and in the analysis, the $T = 5$-min sample is treated as at $T = 0$ min.) Over 150 min, the initially isolated swarmer cells grew in M2G with an initial OD_{600} of 0.3–0.4. For each sample, the cells were treated with 100 μg/mL chloramphenicol for 2 min, rapidly collected by centrifugation, and flash-frozen in liquid nitrogen (6). Lysates were prepared by milling frozen cells in a Retsch mixer mill mm400, as in ref. 6; aliquots were then used for RS and for ribosome profiling.

Ribosome Profiling and RS. RS (11) and RP (6) samples were prepared as described previously, with the exception that the ribozero rRNA extraction kit (Epicentre) was used to subtract rRNA for RS, and the resulting DNA libraries were sequenced on an Illumina HisEq. 2000. Resulting reads were trimmed of the sequencing adapter and aligned to the genome using bowtie 0.12.8 (43). Reads aligning to noncoding genes (tRNAs or rRNAs) were not included in datasets nor considered in the analysis. Read counts are given in the worksheet "Read counts" in Dataset S2.

Ribosome footprints were center-weighted to reflect the position of the decoding center as described by Oh, et al. (44). For the analysis of RS and RP profiles, we quantified transcript levels as RPKM (45). Thus, $RPKM_{nt} = N_{nt}/(len_n/R_t)$ where N_{nt} = number of reads for gene n at time point t, len_n = length of gene n in kilobases, and R_t = total number of non-rRNA/non-tRNA reads in the sample taken at time t in millions). To eliminate data from initiating or terminating ribosomes, the first 10 and last 5 codons were excluded from the RPKM calculation (11, 46). However, for genes with small (fewer than 50 codons) ORFs, the entire length of the ORF was included in the RPKM calculation. For each gene at each time point we calculated the translational efficiency using TE = ribosome $profiling_{RPKM}$/$RNA\text{-}seq_{RPKM}$. The highly unequal distribution of both gene transcription and mRNA translation plus the changing composition and activity of these functions over the cell cycle (Fig. 2) has potential for introducing artifacts when comparing relative activity at different time points. However, our analysis here is focused only on the genes with the strongest temporal TE changes over the cell cycle and the highest RP RPKM, so this not a concern.

The resulting source data used for this paper is in the "Cell cycle expression levels" in Dataset S2, and the data has been deposited in the National Center for Biotechnology Information Gene Expression Omnibus with accession no. GSE68200. In addition, the RS and RP data are installed for visualization using the online CauloBrowser tool (47).

Analysis.

Clustering. The discrete cosine transform (DCT) coefficients for each six-element TE profile vector was calculated, normalized so that the mean of the inverse transform is one. Thus, the first coefficient of the DCT is 1 (the mean)

and the remaining five coefficients contain all of the profile shape information. We then *k*-means–clustered these latter five coefficients to obtain 14 clusters of genes with similar TE temporal profiles (Dataset S1). The same method was used to cluster RP profiles and the resulting clusters are shown in Dataset S3. Because the RP RPKM values are proportional to the protein production rate from each gene at the time of the sampling, these clustered RP profiles give the best available insight into the cell cycle profile of protein production from each gene.

Correlation of antisense transcription start site profiles with the TE profiles. The correlation of cell cycle-regulated antisense transcription start site activity measured by 5′ Global RACE (11) with RS and TE is reported in Dataset S4.

Fluorescent Timers. The fluorescent timer plasmid (pTimerC-4) was generated by fusing sfGFP to the C terminus of a slow-maturing mCherry in the pChyC-4 plasmid. A serine-glycine rich linker fused to sfGFP was inserted downstream of mCherry pChyC-4 (48) using Gibson assembly (49). The PCR products and the PCR primers used in the Gibson assembly reaction are in *SI Appendix*.

The resulting plasmids were sequence-verified and transformed into strain NA1000 by electroporation and selected on PYE Gent plates. NA1000 cell populations harboring the *spmX::Timer* and *B′RNA-pol::Timer* constructs were grown in M2G at 28 °C. Swarmer cells were isolated (41, 42) and allowed to proceed synchronously through the cell cycle. At 30-min intervals we collected 1 μL of cells and imaged them on a 1.5% agarose pad buffered with M2G. To quantify the GFP-to-mCherry signal ratio, we calculated the background subtracted GFP and mCherry intensity using imageJ. The GFP and mCherry ratio was calculated for each cell and the average GFP to mCherry ratio measurements for each time point were obtained for >50 cells.

ACKNOWLEDGMENTS. This work was supported by National Institutes of Health (NIH) (www.nih.gov) postdoctoral fellowship F32 GM100732 to J.M.S., a Jane Coffin Childs Memorial Fund (www.jccfund.org) grant to W.S.C., NIH Grants R01 GM32506 and R35 GM11807101 to L.S., and a Helen Hay Whitney Foundation (www.hhwf.org) Fellowship and NIH Pathway to Independence Award GM105913 to G.-W.L. There was also support from Howard Hughes Medical Institute (www.hhmi.org) to J.S.W., and from National Science Foundation (www.nsf.gov), an Inspire Award CCF-1344284-1 to H.H.M. The funders had no role in study design, data collection and analysis, decision to publish, or preparation of the manuscript.

1. McAdams HH, Shapiro L (2009) System-level design of bacterial cell cycle control. *FEBS Lett* 583(24):3984–3991.
2. McAdams HH, Shapiro L (2011) The architecture and conservation pattern of whole-cell control circuitry. *J Mol Biol* 409(1):28–35.
3. Tsokos CG, Laub MT (2012) Polarity and cell fate asymmetry in *Caulobacter crescentus*. *Curr Opin Microbiol* 15(6):744–750.
4. Collier J (2012) Regulation of chromosomal replication in *Caulobacter crescentus*. *Plasmid* 67(2):76–87.
5. Marks ME, et al. (2010) The genetic basis of laboratory adaptation in *Caulobacter crescentus*. *J Bacteriol* 192(14):3678–3688.
6. Schrader JM, et al. (2014) The coding and noncoding architecture of the *Caulobacter crescentus* genome. *PLoS Genet* 10(7):e1004463.
7. Hottes AK, et al. (2004) Transcriptional profiling of *Caulobacter crescentus* during growth on complex and minimal media. *J Bacteriol* 186(5):1448–1461.
8. Laub MT, McAdams HH, Feldblyum T, Fraser CM, Shapiro L (2000) Global analysis of the genetic network controlling a bacterial cell cycle. *Science* 290(5499):2144–2148.
9. McGrath PT, et al. (2007) High-throughput identification of transcription start sites, conserved promoter motifs and predicted regulons. *Nat Biotechnol* 25(5):584–592.
10. Fang G, et al. (2013) Transcriptomic and phylogenetic analysis of a bacterial cell cycle reveals strong associations between gene co-expression and evolution. *BMC Genomics* 14:450.
11. Zhou B, et al. (2015) The global regulatory architecture of transcription during the *Caulobacter* cell cycle. *PLoS Genet* 11(1):e1004831.
12. Matroule JY, Lam H, Burnette DT, Jacobs-Wagner C (2004) Cytokinesis monitoring during development; rapid pole-to-pole shuttling of a signaling protein by localized kinase and phosphatase in *Caulobacter*. *Cell* 118(5):579–590.
13. Tsokos CG, Perchuk BS, Laub MT (2011) A dynamic complex of signaling proteins uses polar localization to regulate cell-fate asymmetry in *Caulobacter crescentus*. *Dev Cell* 20(3):329–341.
14. Iniesta AA, Shapiro L (2008) A bacterial control circuit integrates polar localization and proteolysis of key regulatory proteins with a phospho-signaling cascade. *Proc Natl Acad Sci USA* 105(43):16602–16607.
15. Childers WS, et al. (2014) Cell fate regulation governed by a repurposed bacterial histidine kinase. *PLoS Biol* 12(10):e1001979.
16. Pyronnet S, Sonenberg N (2001) Cell-cycle-dependent translational control. *Curr Opin Genet Dev* 11(1):13–18.
17. Tanenbaum ME, Stern-Ginossar N, Weissman JS, Vale RD (2015) Regulation of mRNA translation during mitosis. *eLife* 4:4.
18. Stumpf CR, Moreno MV, Olshen AB, Taylor BS, Ruggero D (2013) The translational landscape of the mammalian cell cycle. *Mol Cell* 52(4):574–582.
19. Ingolia NT, Ghaemmaghami S, Newman JR, Weissman JS (2009) Genome-wide analysis in vivo of translation with nucleotide resolution using ribosome profiling. *Science* 324(5924):218–223.
20. Li GW (2015) How do bacteria tune translation efficiency? *Curr Opin Microbiol* 24: 66–71.
21. Li GW, Burkhardt D, Gross C, Weissman JS (2014) Quantifying absolute protein synthesis rates reveals principles underlying allocation of cellular resources. *Cell* 157(3): 624–635.
22. Typas A, Sourjik V (2015) Bacterial protein networks: Properties and functions. *Nat Rev Microbiol* 13(9):559–572.
23. Quax TE, et al. (2013) Differential translation tunes uneven production of operon-encoded proteins. *Cell Reports* 4(5):938–944.
24. Ingolia NT, Brar GA, Rouskin S, McGeachy AM, Weissman JS (2012) The ribosome profiling strategy for monitoring translation in vivo by deep sequencing of ribosome-protected mRNA fragments. *Nat Protoc* 7(8):1534–1550.
25. Jiang C, Brown PJ, Ducret A, Brun YV (2014) Sequential evolution of bacterial morphology by co-option of a developmental regulator. *Nature* 506(7489):489–493.
26. Hughes HV, et al. (2010) Protein localization and dynamics within a bacterial organelle. *Proc Natl Acad Sci USA* 107(12):5599–5604.
27. Goley ED, et al. (2011) Assembly of the *Caulobacter* cell division machine. *Mol Microbiol* 80(6):1680–1698.
28. Bowman GR, et al. (2010) *Caulobacter* PopZ forms a polar subdomain dictating sequential changes in pole composition and function. *Mol Microbiol* 76(1):173–189.
29. Lam H, Matroule JY, Jacobs-Wagner C (2003) The asymmetric spatial distribution of bacterial signal transduction proteins coordinates cell cycle events. *Dev Cell* 5(1): 149–159.
30. Radhakrishnan SK, Thanbichler M, Viollier PH (2008) The dynamic interplay between a cell fate determinant and a lysozyme homolog drives the asymmetric division cycle of *Caulobacter crescentus*. *Genes Dev* 22(2):212–225.
31. Thanbichler M, Shapiro L (2006) MipZ, a spatial regulator coordinating chromosome segregation with cell division in *Caulobacter*. *Cell* 126(1):147–162.
32. Khmelinskii A, et al. (2012) Tandem fluorescent protein timers for in vivo analysis of protein dynamics. *Nat Biotechnol* 30(7):708–714.
33. Duval M, Simonetti A, Caldelari I, Marzi S (2015) Multiple ways to regulate translation initiation in bacteria: Mechanisms, regulatory circuits, dynamics. *Biochimie* 114:18–29.
34. Sauert M, Temmel H, Moll I (2015) Heterogeneity of the translational machinery: Variations on a common theme. *Biochimie* 114:39–47.
35. Gingold H, Dahan O, Pilpel Y (2012) Dynamic changes in translational efficiency are deduced from codon usage of the transcriptome. *Nucleic Acids Res* 40(20): 10053–10063.
36. McAdams HH, Shapiro L (2003) A bacterial cell-cycle regulatory network operating in time and space. *Science* 301(5641):1874–1877.
37. Qin X, Sarnow P (2004) Preferential translation of internal ribosome entry site-containing mRNAs during the mitotic cycle in mammalian cells. *J Biol Chem* 279(14): 13721–13728.
38. Pyronnet S, Pradayrol L, Sonenberg N (2000) A cell cycle-dependent internal ribosome entry site. *Mol Cell* 5(4):607–616.
39. Tedin K, et al. (1999) Translation initiation factor 3 antagonizes authentic start codon selection on leaderless mRNAs. *Mol Microbiol* 31(1):67–77.
40. Moll I, Grill S, Gualerzi CO, Bläsi U (2002) Leaderless mRNAs in bacteria: Surprises in ribosomal recruitment and translational control. *Mol Microbiol* 43(1):239–246.
41. Schrader JM, Shapiro L (2015) Synchronization of *Caulobacter crescentus* for investigation of the bacterial cell cycle. *J Vis Exp* (98):e52633.
42. Evinger M, Agabian N (1977) Envelope-associated nucleoid from *Caulobacter crescentus* stalked and swarmer cells. *J Bacteriol* 132(1):294–301.
43. Langmead B, Trapnell C, Pop M, Salzberg SL (2009) Ultrafast and memory-efficient alignment of short DNA sequences to the human genome. *Genome Biol* 10(3):R25.
44. Oh E, et al. (2011) Selective ribosome profiling reveals the cotranslational chaperone action of trigger factor in vivo. *Cell* 147(6):1295–1308.
45. Mortazavi A, Williams BA, McCue K, Schaeffer L, Wold B (2008) Mapping and quantifying mammalian transcriptomes by RNA-Seq. *Nat Methods* 5(7):621–628.
46. Li G-W, Oh E, Weissman JS (2012) The anti-Shine-Dalgarno sequence drives translational pausing and codon choice in bacteria. *Nature* 484(7395):538–541.
47. Lasker K, et al. (2016) CauloBrowser: A systems biology resource for Caulobacter crescentus. *Nucleic Acids Res* 44(D1):D640–D645.
48. Thanbichler M, Iniesta AA, Shapiro L (2007) A comprehensive set of plasmids for vanillate- and xylose-inducible gene expression in *Caulobacter crescentus*. *Nucleic Acids Res* 35(20):e137.
49. Gibson DG, et al. (2009) Enzymatic assembly of DNA molecules up to several hundred kilobases. *Nat Methods* 6(5):343–345.